Supplemental to *Validation of MAX-DOAS retrievals of aerosol extinction, SO_2 and NO_2 through comparison with lidar, sun photometer, Active-DOAS and aircraft measurements in the Athabasca Oil Sands Region.*

Section 1 Emissions of NO_2 and SO_2 from AOSR Industrial Facilities

Table S1 Annual Emissions NO_2 in kilotonnes from select facilities.

Facility	NPRI 2013	Off-road vehicle & tail-pipe emissions (Zhang et al., 2018) from 2010	Stack & area sources (Zhang et al., 2018) (2012-2013 period)
Syncrude Mildred Lake Plant	14	8.0	14
Suncor Millennium Plant/Steepbank	8	10.7	11.5
Shell Muskeg River/Jackpine	1.3	7.0	0.7
CNRL Horizon	1.5	5.6	1.8
Imperial Oil Kearl	0.3	1.3	0

Table S2 Annual Emissions SO_2 in kilotonnes from select facilities.

Facility	NPRI 2013	Off-road vehicle & tail-pipe emissions (Zhang et al., 2018) from 2010	Stack & area sources (Zhang et al., 2018) (2012-2013 period)
Syncrude Mildred Lake Plant	63	0.36	77
Suncor Millennium Plant/Steepbank	14	0.06	21
Shell Muskeg River/Jackpine	0	0.13	0
CNRL Horizon	4	0.07	6.5
Imperial Oil Kearl	0	0.03	0

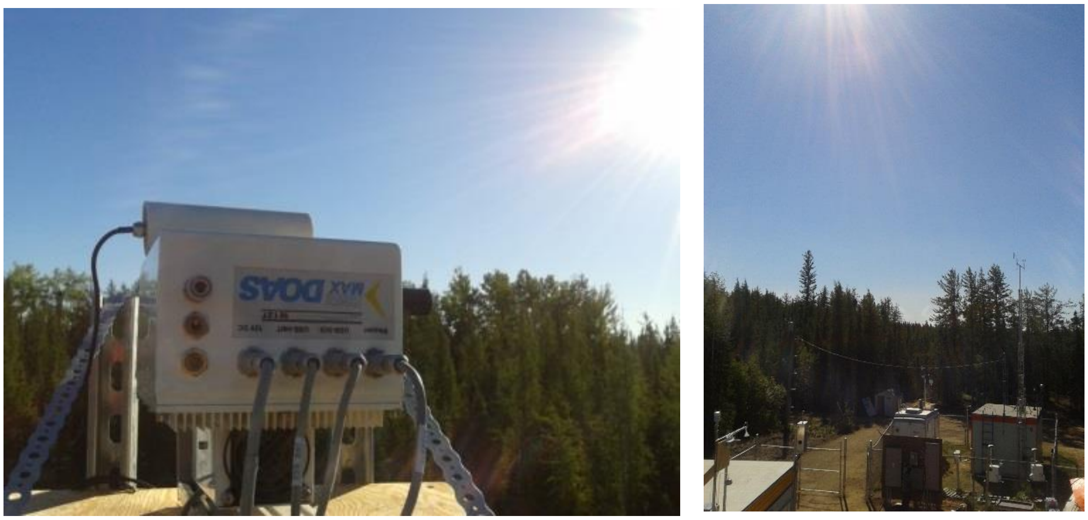

Figure S1 The MAX-DOAS instrument mounted at 5 m a.gl. (left) at Fort McKay South and the view South of the instrument.

Section 2 Additional Information on MAX-DOAS Spectral Fitting

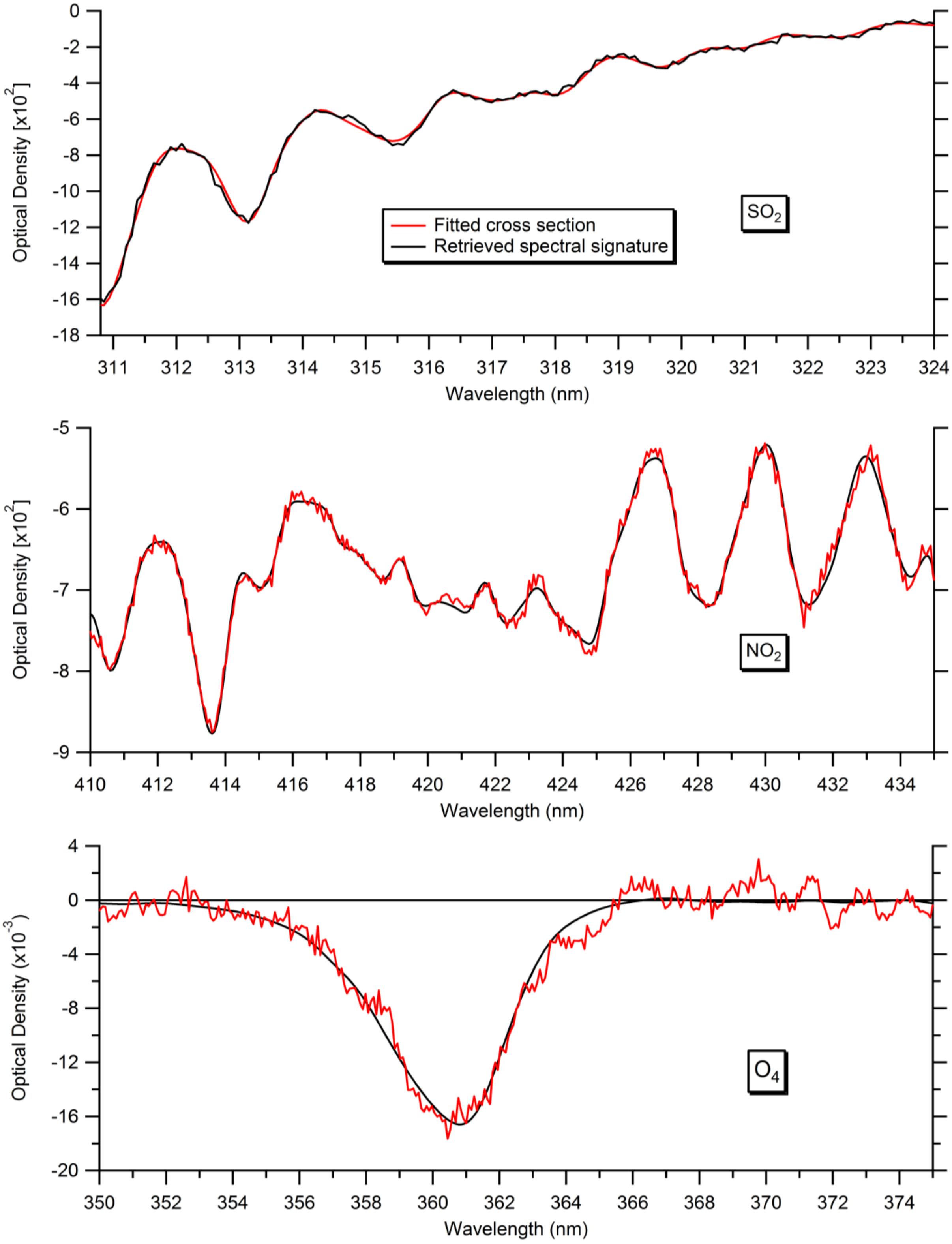

Figure S2 Examples of spectral retrievals of SO_2, NO_2 and O_4 Retrieved dSCDs were 5.79(+/-0.09)x10^{17} molec cm^{-2}, 1.2(+/-0.01)x10^{17} molec cm^{-2}, and 3.96(+/-0.08)x10^{43} molec cm^{-2}, respectively. The spectra were measured under clear sky conditions at 2^o in 2013 at 22:37 UTC on Aug 23 and 18:34 UTC on Sep 04, respectively.

SO_2 Spectral Fitting Experiments with Calibration Gas Cell

A SO_2 gas cell with a slant column density (SCD) of $2.2e^{17}$ (+/- 10%) molecules cm^{-2} was placed inside the MAX-DOAS telescope tube. Scattered solar light spectra were recorded around solar noon at viewing elevation angles of 2^o, 4^o, 8^o, 30^o and 90^o above the horizon, followed by a 90^o measurement without the gas cell. This second zenith measurement was used as the FRS. Active-DOAS measurements of the SO_2 gas cell confirmed the SCD. dSCDs of SO_2 were fit in DOASIS with varying fitting windows using a lower limit range of 303-318 nm and an upper limit range of 309-340 nm in ~0.3 nm increments. The fit components can be found in Table 2.

Fitting SO_2 in the measured wavelength region is challenging because the SO_2 absorption features (Fig. S3) are strongest where the measured light intensity was small, and the influence of stray light can be large. Increasing O_3 absorption at decreasing wavelengths approaching 300 nm reduces the spectral signal. The lower limit wavelength of the fitting window must balance including strong SO_2 features and enough signal intensity. The upper limit wavelength should ensure that the fitting window includes as many SO_2 absorption features as possible while excluding wavelengths where SO_2 absorption features are so weak that degrees of freedom and fitting uncertainty are increased.

dSCD of SO_2 fitted from the spectra measured at elevation angles closer to horizon-pointing exhibited fewer wavelength fitting windows where the fitted dSCD was within +/-15% of the expected value. Spectra measured at lower elevation angles had less UV signal because the longer light path lengths closer to the ground experience more Rayleigh scattering that preferentially scattered away shorter wavelengths. Since the visible light intensity remains the same and is a source of stray light, the reduced UV signal increased the impact of stray light on the dSCD (signal to noise ratio decreases). Stray light artificially increases the measured intensity and tends to cause underestimation of the retrieved dSCD.

Stray light has the largest impact on the signal at the lowest wavelengths where the measured intensity was the lowest. Stray light interference is apparent in the frequent underestimation of the dSCD for the 2^o spectrum with fitting windows with lower limits <307 nm (gray datapoints in Fig. S4). The dSCDs were often >15% less than the expected value for fitting windows with a lower limit <308 nm, particularly for the lower elevation angles. The fitted dSCD was sensitive to small changes in the fitting window for lower limits <308 nm and upper limit <330 nm, changing up to ~20% change for a 0.5 nm difference in the lower limit (Figs. S4 & S5). The fitted dSCD is inversely proportion to the SO_2 absorption cross section (Fig S4). When the strongest SO_2 absorption feature included in the fit was an absorption maximum, the measured intensity in lowest wavelength region was even further reduced, leading to up to a 25% reduction in the dSCD compared to a window where the adjacent absorption minimum was the strongest feature included (Fig. S5). This result implies that small errors in the wavelength calibration or wavelength shift could significantly deviate the dSCD from the true value. dSCDs exhibited less dependence on the lower limit for windows with lower limit wavelengths of 310.4-311 nm due to increased signal intensity. For lower limit wavelengths >312 nm, the SO_2 absorption features are substantially weaker, leading to dSCDs that tended to be >15% larger than the expected value and varied significantly with relatively small changes in higher limit wavelength (Fig. S4). Since the SO_2 absorption features after 324 nm are very weak, the fitting range upper limit was set to 324 nm.

Based on these results, an SO_2 fitting range of 310.5-324 nm was chosen for this instrument.

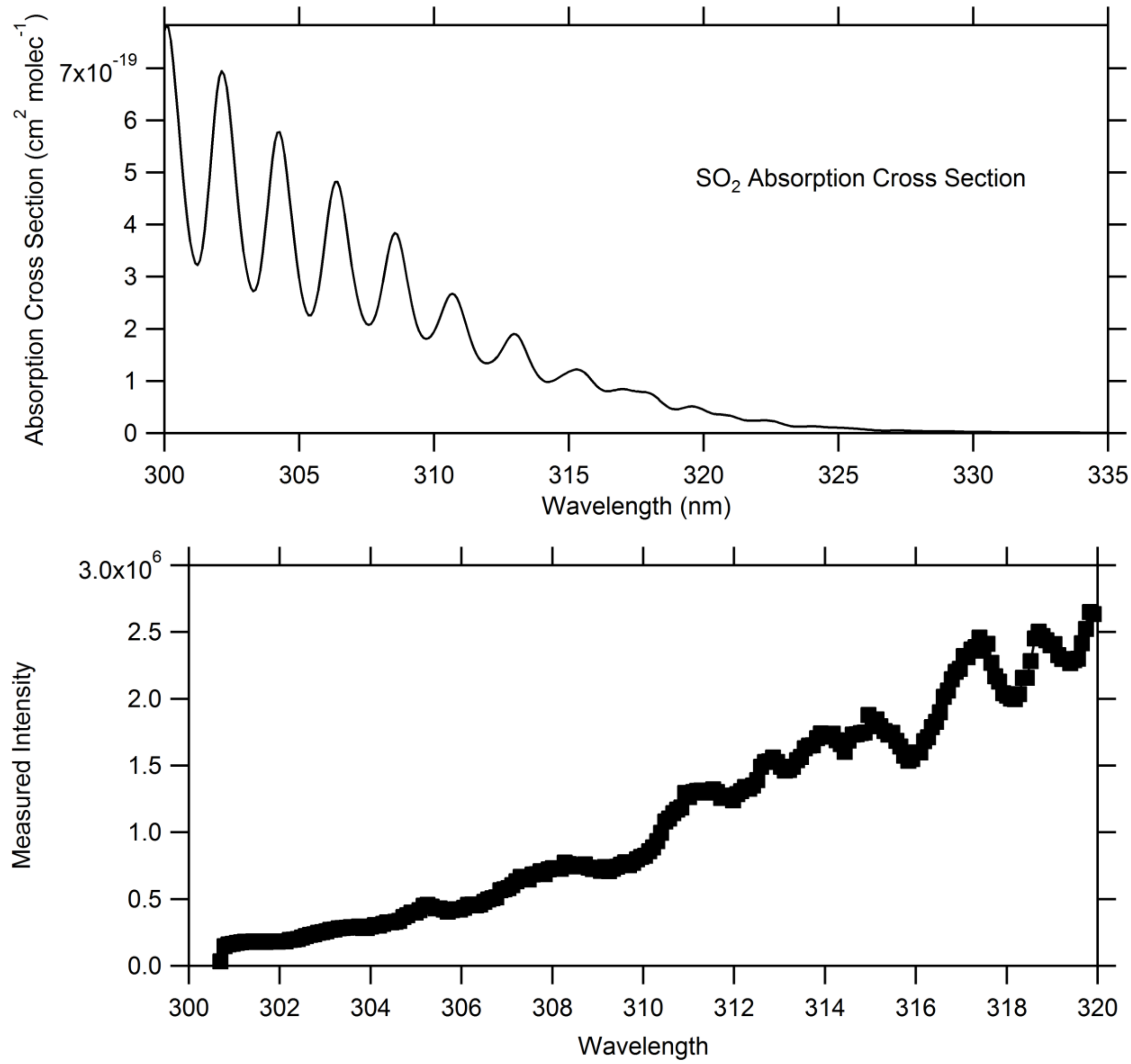

Figure S3 SO_2 Absorption Cross Section (top) and Measured Intensity from the 2° Spectrum from 300-320 nm (bottom).

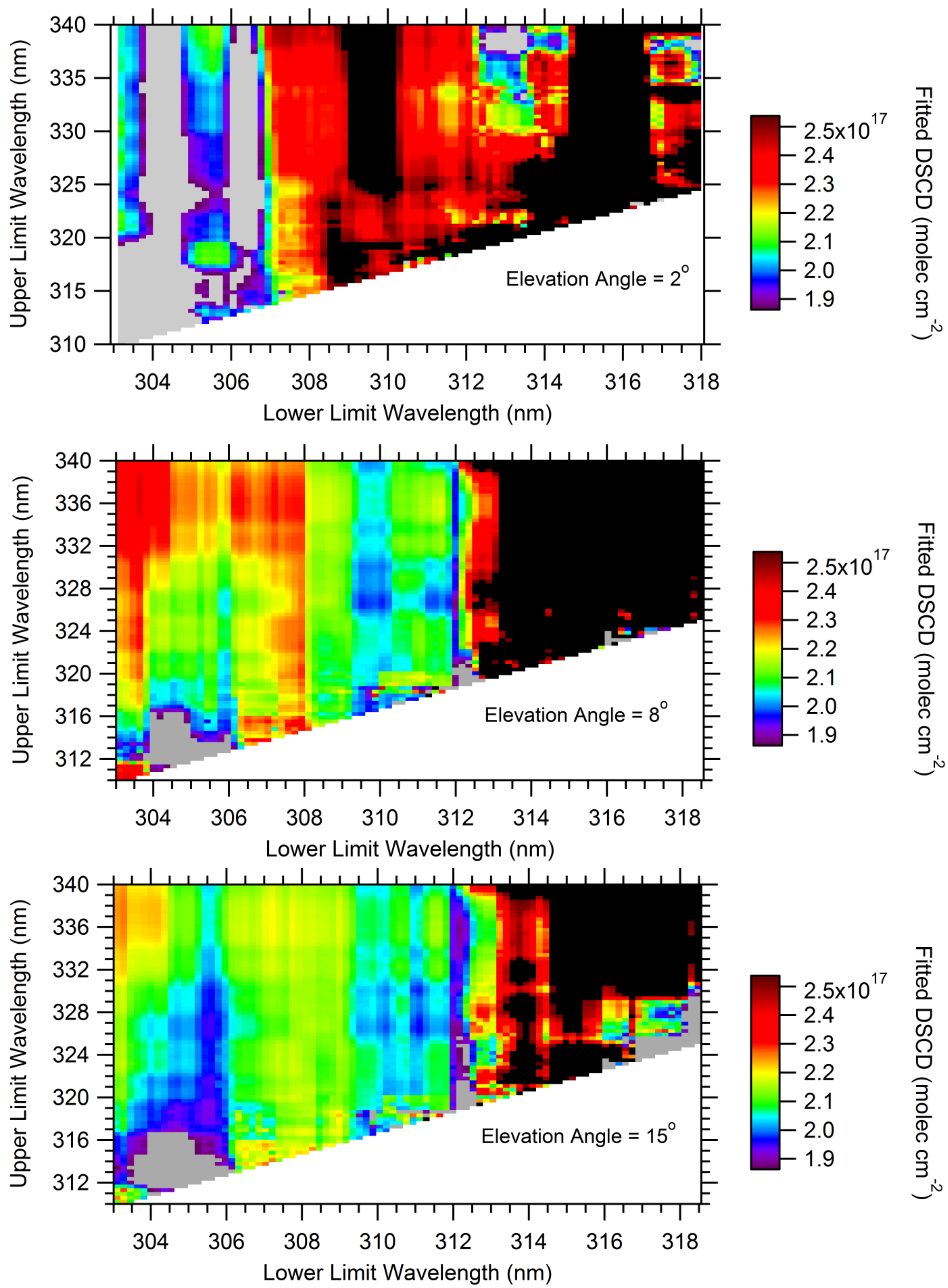

Figure S4 dSCDs of SO2.2.2x10^{17} molecules cm^{-2} gas cell using varying spectral fitting ranges. Gray and black datapoints indicate that the fitted dSCD was 15% less than and greater than 2.2x10^{17} molec cm^{-2}, respectively.

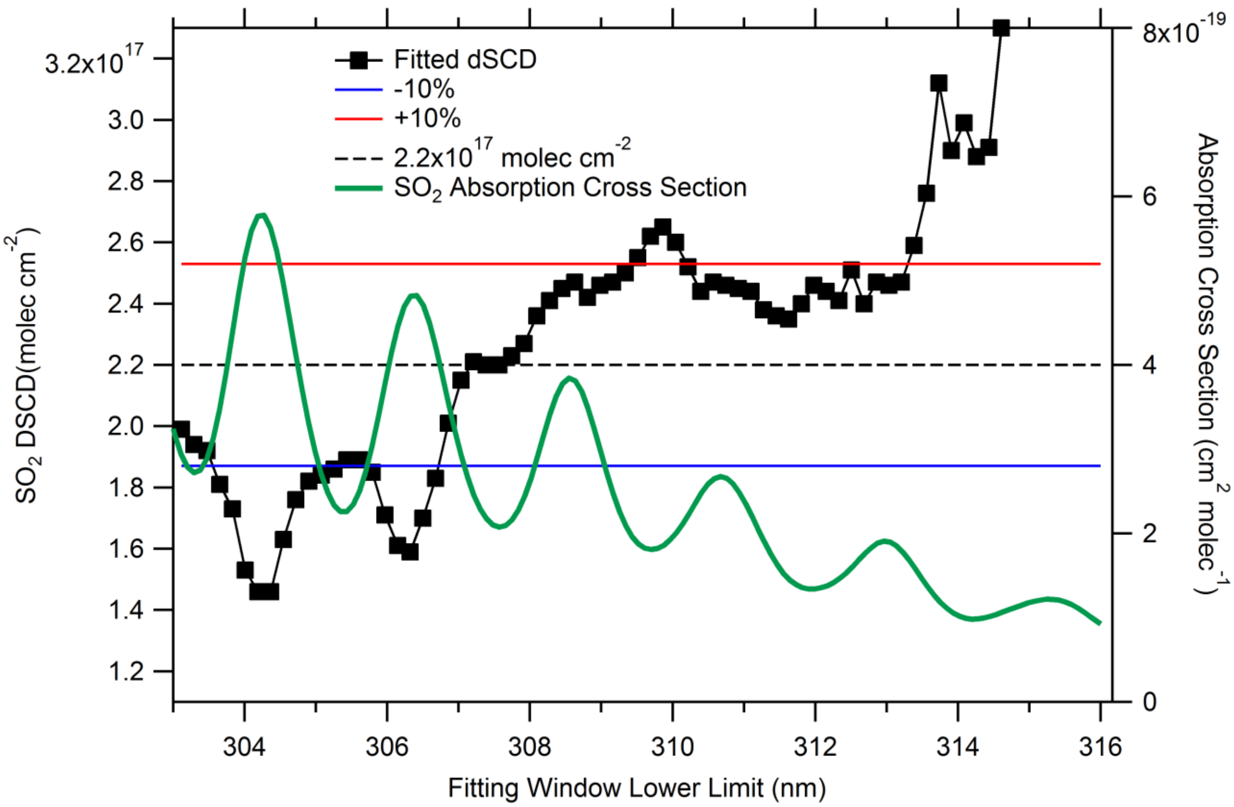

Figure S5 Fitted dSCD of SO_2 with fitting window upper limit of 320 nm from 2^o Spectrum using a $2.2x10^{17}$ molec cm^{-2} gas cell (black trace) and SO_2 absorption cross section degraded to the spectrometer's resolution (green trace).

Section 3 Lidar S-ratio Measurements in the AOSR

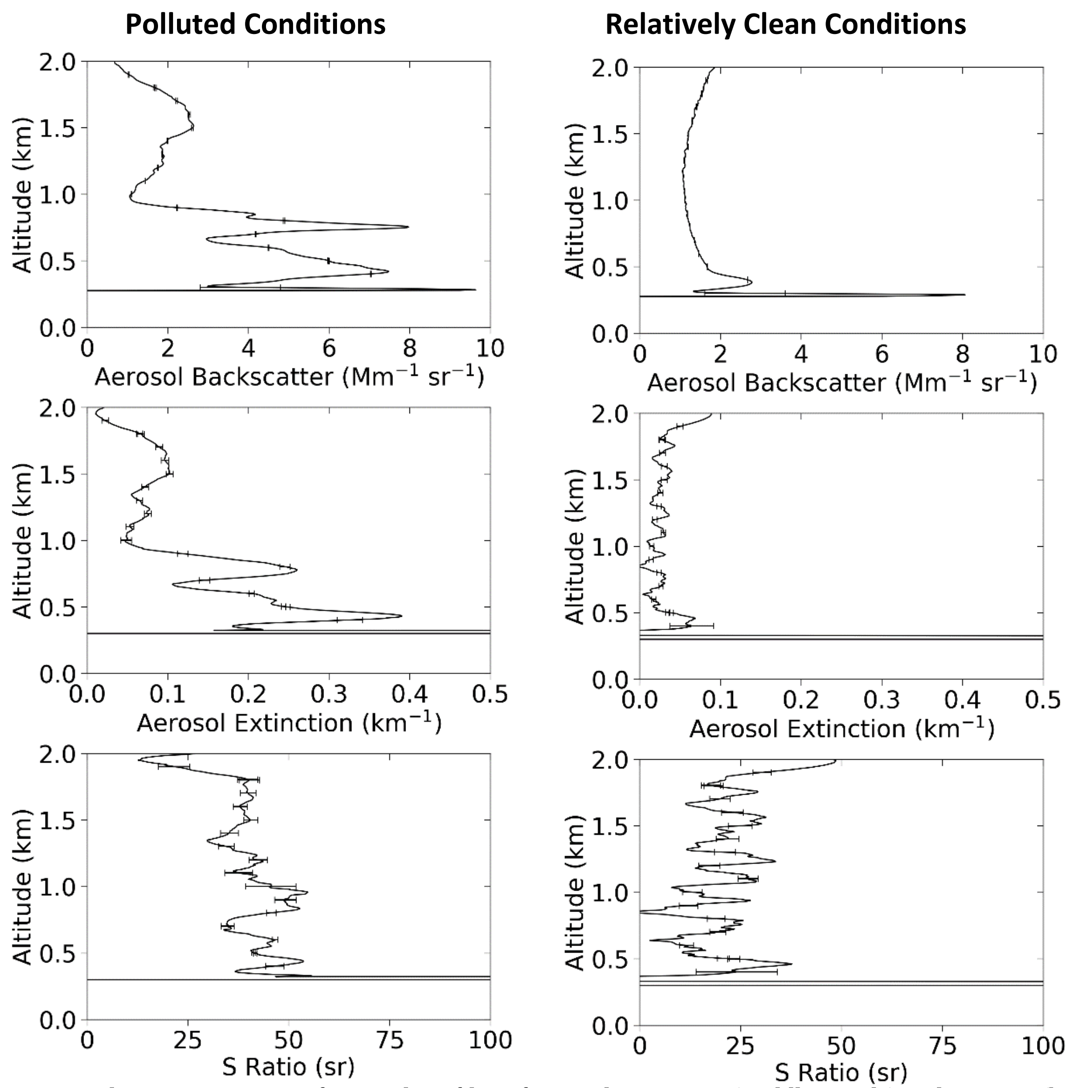

Figure S6 Lidar measurements of vertical profiles of aerosol extinction (middle panels) and S-ratios (bottom panels) under polluted conditions (left column) and relatively clean conditions (right column) at Oski-Ôtin in 2018.

Section 4 Linear Regression Statistics

Table S3 Aug 23 AOD Linear Regressions.

Y	MAX-DOAS AOD	MAX-DOAS AOD	MAX-DOAS AOD	MAX-DOAS AOD	AERONET AOD -30 mins	AERONET AOD -30 mins
X	AERONET AOD -30mins	AERONET AOD	Lidar AOD S=50 sr in plume	Lidar AOD S=25 sr	Lidar S=50 sr	Lidar S=25 sr
Slope	0.98±0.02	1.03±0.01	1.15±0.02	2.18±0.03	1.08±0.02	2.18±0.01
Intercept	-0.08±0.00	-0.07±0.00	-0.01±0.00	-0.06±0.00	0.07±0.00	0.03±0.01
R^2	0.92	0.80	0.97	0.97	0.98	0.96
N	21	23	21	24	22	22

Table S4 Aug 23 trace-gas linear regressions. *Denotes the matrix was near-singular or badly conditioned; statistical results may be inaccurate.

Y	MAX-DOAS SO_2 VCD	MAX-DOAS SO_2 VCD	MAX-DOAS NO_2 VCD	MAX-DOAS NO_2 VCD	WBEA Fort McKay South SO_2 mixing ratio	WBEA Fort McKay South NO_2 mixing ratio
X	Pandora SO_2 VCD	Pandora SO_2 VCD -30mins	Pandora NO_2 VCD	Pandora NO_2 VCD -30 mins	WBEA Oski-Ôtin SO_2 mixing ratio - 30 mins	WBEA Oski-Ôtin NO_2 mixing ratio - 30 mins
Slope	*1.61±0.10	*1.55±0.07	*2.03±0.07	*2.20±0.07	1.42±0.05	1.93±0.07
Intercept	*$1.50x10^{16}$±$0.25x10^{16}$	*$1.16x10^{16}$±$0.24x10^{16}$	*-4.56^{15}±$0.51x10^{15}$	*-$6.36x10^{15}$±$0.56x10^{15}$	0.50±0.01	1.95±0.52
R^2	0.51	0.82	0.68	0.87	0.91	0.61
N	24	23	24	23	109	109

Table S5 Sep 03 AOD and trace-gas linear regressions for data from 11:30 to 18:00. ^Denotes that one or both variables exhibited little variation; the R^2 is not interpretable.

Y	MAX-DOAS AOD	MAX-DOAS AOD	AERONET AOD	MAX-DOAS SO_2 VCD	MAX-DOAS NO_2 VCD	WBEA Fort McKay South SO_2 mixing ratio	WBEA Fort McKay South NO_2 mixing ratio
X	AERONET AOD	Lidar AOD	Lidar AOD	Pandora SO_2 VCD	Pandora NO_2 VCD	WBEA Oski-Ôtin SO_2 mixing ratio	WBEA Oski-Ôtin NO_2 mixing ratio
Slope	0.01±0.01	-0.59±0.36	3.30±0.48	5.27±2.9	-0.19±0.64	0.97±0.10	0.61±0.08
Intercept	-0.01±0.01	0.12±0.02	-0.08±0.03	$-1.5 \times 10^{17} \pm 1.11 \times 10^{17}$	$1.38 \times 10^{16} \pm 0.44 \times 10^{15}$	-1.91±1.99	1.82±0.53
R^2	^0.02	^0.05	^0.47	^0.01	^0.00	0.53	0.38
N	16	16	16	13	12	80	80

Table S6 Sep 04 AOD and trace-gas linear regressions. *Denotes the matrix was near-singular or badly conditioned; statistical results may be inaccurate. . ^Denotes that one or both variables exhibited little variation; the R^2 is not interpretable.

Y	MAX-DOAS AOD	MAX-DOAS AOD	AERONET AOD	MAX-DOAS SO_2 VCD	MAX-DOAS NO_2	WBEA Fort McKay South SO_2 mixing ratio	WBEA Fort McKay South NO_2 mixing ratio
X	AERONET AOD	Lidar AOD	Lidar AOD	Pandora SO_2 VCD	Pandora NO_2 VCD	WBEA Bertha Ganterfort SO_2 mixing ratio	WBEA Bertha Ganterfort NO_2 mixing ratio
Slope	0.39±0.031	0.78±0.08	2.23±0.07	1.10±0.33	*0.95±0.07	0.58±0.04	0.86±0.02
Intercept	-0.01±0.01	0.00±0.01	0.02±0.01	$4.62 \times 10^{15} \pm 2.40 \times 10^{15}$	$*9.44 \times 10^{14} \pm 3.93 \times 10^{14}$	1.77±0.25	1.00±0.16
R^2	0.31	0.20	0.91	0.51	0.85	0.7	0.92
N	25	25	25	25	25	108	108

Table S7 Sep 05 AOD linear regressions.

Y	MAX-DOAS AOD	MAX-DOAS AOD	AERONET AOD
X	AERONET AOD	Lidar AOD	Lidar AOD
Slope	1.04±0.08	2.94±0.38	3.24±0.15
Intercept	-0.08±0.01	-0.10±0.02	-0.03±0.01
R^2	0.77	0.51	0.89
N	26	20	20

Table S8 Sep 06 AOD linear regressions. *Denotes the matrix was near-singular or badly conditioned; statistical results may be inaccurate. ^Denotes that one or both variables exhibited little variation; the R^2 is not interpretable.

Y	MAX-DOAS AOD	MAX-DOAS AOD	AERONET AOD 361
X	AERONET AOD	Lidar AOD	Lidar AOD
Slope	*-2.01±0.93	5.56±1.27	-2.33±0.73
Intercept	0.24±0.09	-0.21±0.06	0.20±0.03
R^2	^0.02	0.02	^0.08
N	24	23	23

Table S9 Sep 07 AOD and trace-gas linear regressions. *Denotes the matrix was near-singular or badly conditioned; statistical results may be inaccurate.

Y	MAX-DOAS AOD	MAX-DOAS AOD	AERONET AOD	MAX-DOAS SO_2 VCD	MAX-DOAS NO_2 VCD	WBEA Fort McKay South SO_2 mixing ratio	WBEA Fort McKay South NO_2 mixing ratio
X	AERONET AOD	Lidar AOD	Lidar AOD	Pandora SO_2 VCD	Pandora NO_2 VCD	WBEA Bertha Ganterfort SO_2 mixing ratio	WBEA Bertha Ganterfort NO_2 mixing ratio
Slope	0.73±0.06	1.83±0.13	2.34±0.10	*$1.48x10^{14}±1.48x10^{14}$	*1.53±3.3	0.99±0.07	1.06±0.03
Intercept	-0.03±0.01	-0.04±0.01	0.00±0.00	*-$1.09x10^{30}±1.049x10^{30}$	*$4.10x10^{15}±1.75x10^{16}$	-0.04±0.36	1.05±0.23
R^2	0.64	0.67	0.55	^0.00	^0.05	0.64	0.90
N	26	26	26	26	26	108	108

Section 5 Example of Averaging Kernel Matrix from MAX-DOAS Optimal Estimation Retrieval

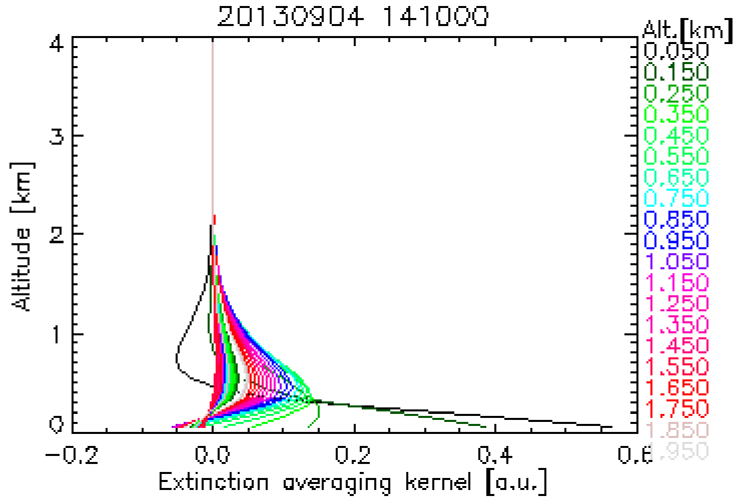

Figure S7 Example of typical averaging kernels from the MAX-DOAS Sep 04 14:10 retrieval of aerosol extinction.

Section 6 Detailed Plots of Selected Lidar Data

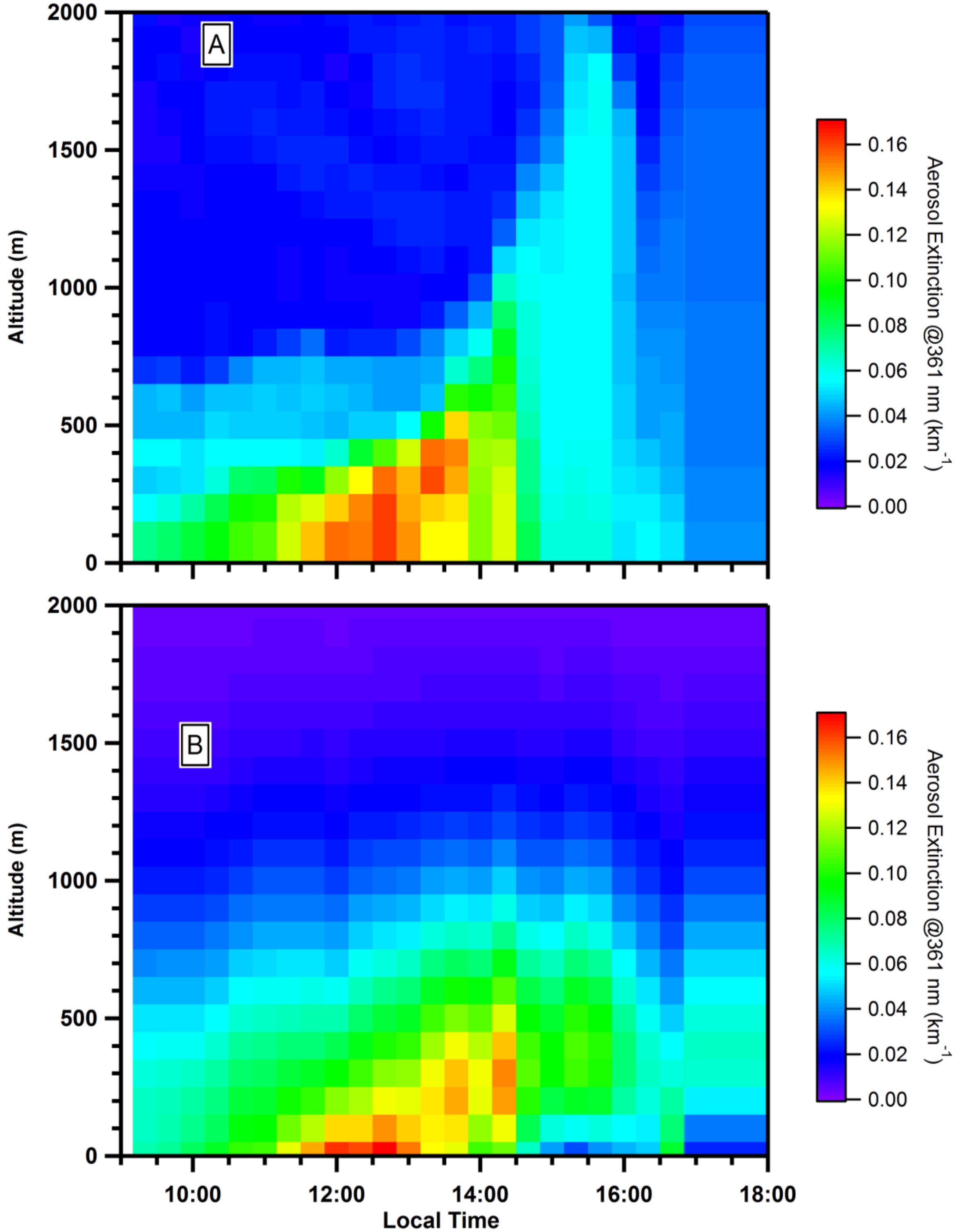

Figure S8 Detail of Sep 04 averaged (A) and smoothed (B) lidar profiles from 0-2 km.

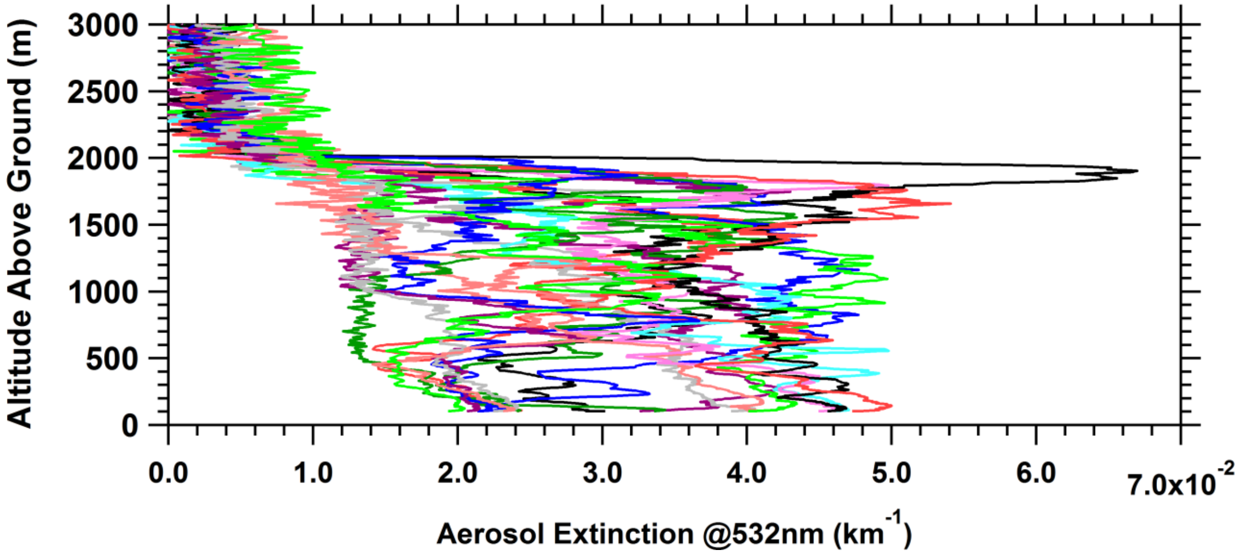

Figure S9 Variability in lidar vertical profiles of aerosol extinction from 15:27 to 15:37 local time on Sep 07.

Section 7 WBEA In-Situ Measurements of SO_2 and NO_2 at For McKay South and Fort McKay Sites

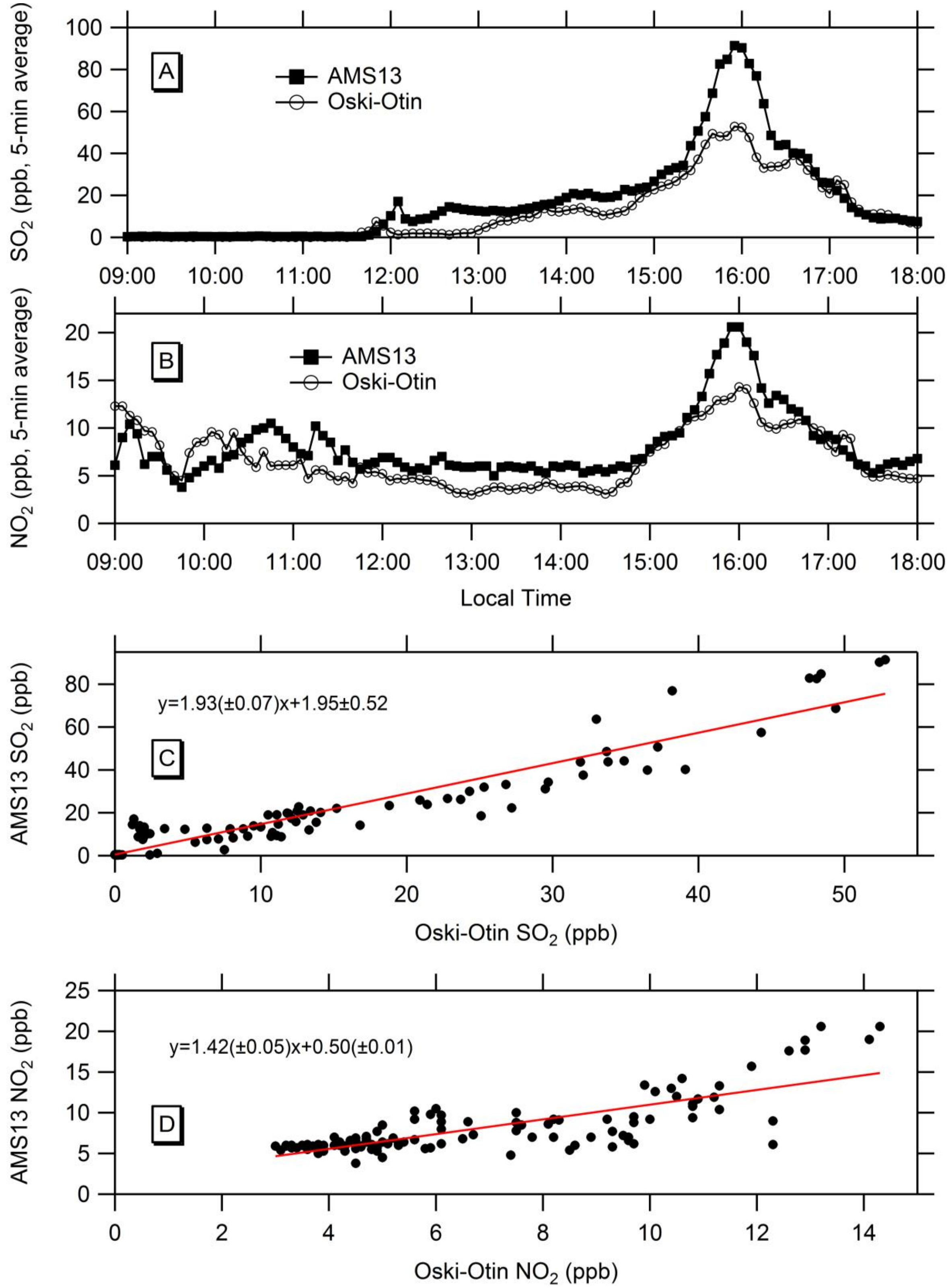

Figure S10 Aug 23 Time series of 5-minute average mixing ratios of SO_2 (A) and NO_2 (B) at Fort McKay South and Oski-Ôtin and linear regression scatter plots for SO_2 (C) and NO_2 (D).

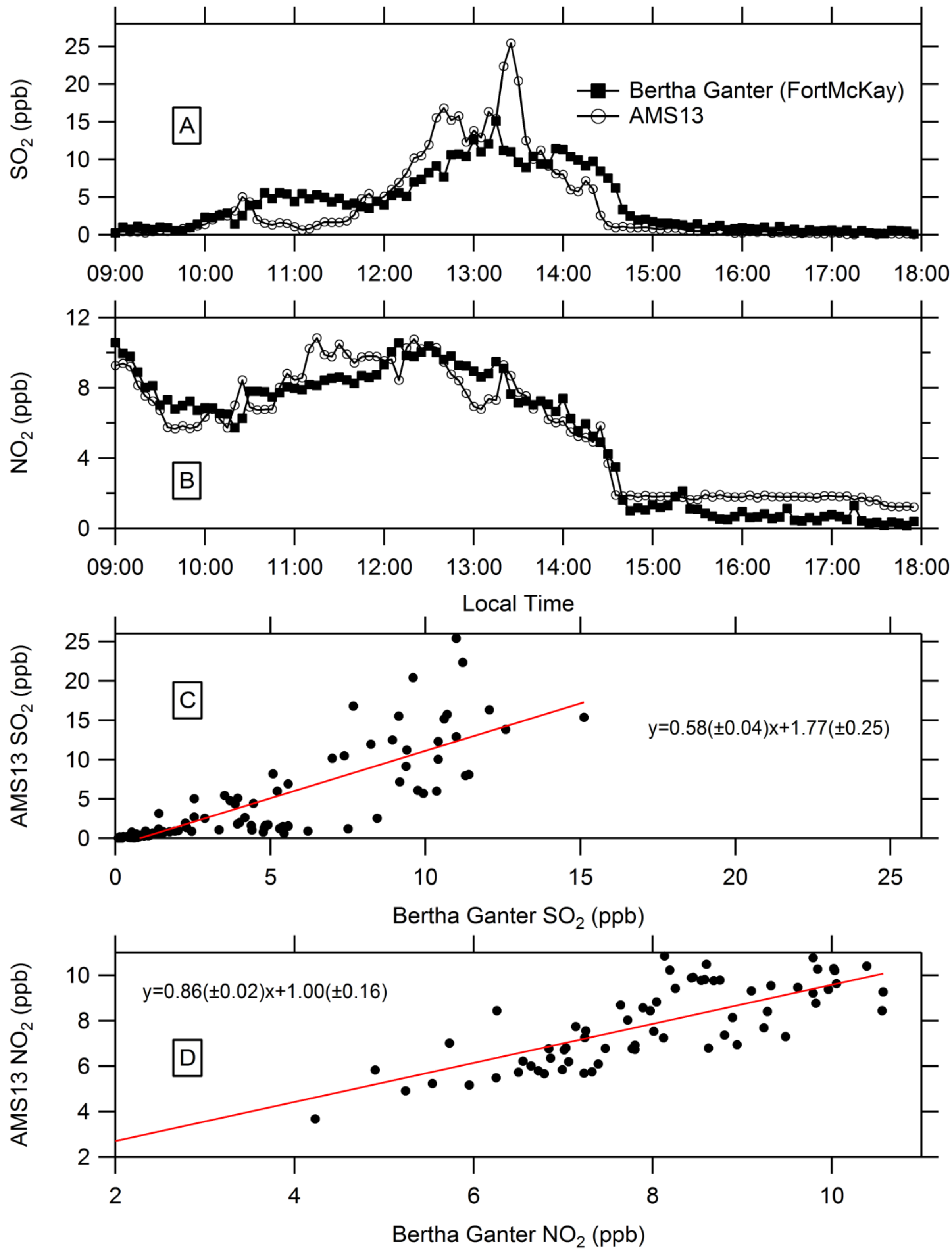

Figure S11 Sep 04 Time series of 5-minute average mixing ratios of SO_2 (A) and NO_2 (B) at Fort McKay South and Oski-Ôtin and linear regression scatter plots for SO_2 (C) and NO_2 (D).